Organic Electronics 13 (2012) 36–42

Contents lists available at SciVerse ScienceDirect

Organic Electronics

journal homepage: www.elsevier.com/locate/orgel

Photoconductivity anisotropy study in uniaxially aligned polymer based planar photodiodes

Dhritiman Gupta [a,1], Thomas J.K. Brenner [a], Sebastian Albert-Seifried [a], Mi Jung Lee [a,2], Martin Heeney [b], Iain McCulloch [b], Henning Sirringhaus [a,*]

[a] Cavendish Laboratory, University of Cambridge, JJ Thomson Avenue, Cambridge CB3 0HE, United Kingdom
[b] Department of Chemistry, Imperial College of London, London SW7 2AZ, United Kingdom

ARTICLE INFO

Article history:
Received 13 June 2011
Received in revised form 10 August 2011
Accepted 16 August 2011
Available online 18 October 2011

Keywords:
Uniaxial polymer alignment
Photoconductivity anisotropy
Photoconductive gain
Donor/acceptor bilayer
Transient response

ABSTRACT

A study of photoconductivity in a planar photodiode based on the uniaxially aligned, semi-crystalline polymer, poly(2,5-bis(3-alkylthiophene-2-yl)thieno[3,2-b]thiophene) (PBTTT) is presented. The charge carrier photogeneration yield in bulk conjugated polymers is usually low but it could possibly be enhanced by applying a sufficiently large electric field, particularly along the direction of the polymer backbone. PBTTT is, in principle, an ideal system to study any anisotropy in carrier photogeneration because directional alignment of fully extended polymer chains can be achieved over macroscopic length scales. However, we have found that electron trapping in this polymer results in high photoconductive gain obscuring measurements of intrinsic photogeneration. We study the mechanism of photoconductive gain using steady-state and transient photocurrent measurement. Constant background illumination and the deposition of a surface layer of an electron acceptor material have been found to be effective in reducing the gain effects.

1. Introduction

Over the past two decades organic solar cells based on donor–acceptor bulk heterojunctions of polymer–fullerene [1], polymer–polymer [2,3] and polymer–nanoparticle [4] blends have been utilized to facilitate the charge generation processes from the primary photogenerated excitons. Despite suffering a significant energy loss at the heterojunction during the charge transfer process and a consequent reduction in open circuit voltage [5,6], this technology has become quite successful and more than 7–8% solar cell efficiency has been demonstrated [1]. The donor–acceptor heterojunction architecture is indispensible at the moment since photogeneration in pristine polymers is significantly lower owing to the large exciton binding energy. However, recently it has been claimed that in films of pristine poly-3-hexylthiophene, almost 15% of the absorbed photons give rise to direct generation of free charge carriers while 85% give rise to excitons following the photoexcitation process [7,8].

In order to understand better the mechanisms for charge carrier generation in pristine polymers it is interesting to investigate whether charge generation depends on the alignment of the polymer chains with respect to an externally applied electric field. In a uniaxially aligned polymer film it might be easier to separate photogenerated excitons into free charge carriers if the electric field is aligned parallel to the chain alignment direction, along which the charge carrier mobility tends to be higher and the exciton state is expected to be more polarizable than in the direction perpendicular to the chain direction. Faster intrachain transport might help the electrons and holes to get swept apart quickly and move out from their mutual Coulomb capture radius to escape recombination. In previous reports on aligned

* Corresponding author. Tel.: +44 01223 337557; fax: +44 01223 337706.
E-mail address: hs220@cam.ac.uk (H. Sirringhaus).
[1] Present address: Molecular Materials and Nanosystems, Department of Chemical Engineering and Chemistry, Eindhoven University of Technology, P.O. Box 513, 5600 MB Eindhoven, Netherlands.
[2] Present address: School of Advanced Materials Engineering, Kookmin University, Seoul, South Korea.

1566-1199/$ - see front matter © 2011 Elsevier B.V. All rights reserved.
doi:10.1016/j.orgel.2011.08.034

light-emitting polymer field-effect transistors it was found that non-geminate recombination is reduced significantly when chains are aligned along the field direction [9,10].

The semicrystalline polymer, poly(2,5-bis(3-alkylthiophene-2-yl)thieno[3,2-b]thiophene) (PBTTT), has recently drawn much attention due to its high charge carrier mobility in transistor devices, higher environmental stability and higher structural order as compared to other polythiophene materials [11]. Fused thiophene rings give rise to a rigid rod structure and the increased separation distance between the alkyl side chains facilitates dense side-chain interdigitation and high degree of ordering. Thin films of PBTTT, annealed above a second phase transition temperature at ~250 °C, exhibit nanometer wide ribbon-like morphology, in which the polymer chains are fully extended. Nanoribbons are formed with edge on stacking of the PBTTT chains with a characteristic width of 70–80 nm, which is consistent with the length of the fully extended polymer chain backbone as calculated from the molecular weight of the polymer. The nanoribbons extend over microns in the direction of the π–π stacking. Due to its well ordered microstructure, uniaxially aligned films of PBTTT should be an ideal system to study any anisotropy in the charge photogeneration in conjugated polymers.

Uniaxial alignment of the nanoribbons can be achieved by directional flow coating methods where the nanoribbons become oriented perpendicular to the flow direction [12]. We have also been able to align films of PBTTT uniaxially using the zone-casting method as reported previously [13]. In this technique a polymer solution at a controlled temperature is pushed through a linear nozzle and the meniscus is moved slowly along the substrate held at a slightly higher temperature to induce directed crystallization of the organic semiconductor on the substrate. Highly aligned PBTTT nanoribbons are achieved using this technique. Here we investigate planar photodiodes fabricated by evaporating two top contacts on top of such aligned PBTTT films. This geometry should allow us to compare the charge generation efficiency with two different orientations of the applied field, parallel to the polymer chain direction and perpendicular to it.

Even though a significant mobility anisotropy was achieved, in this system, electron trapping and high dark current were limiting factors in this device geometry. These gave rise to high photoconductive gain obscuring the measurement of the "actual" anisotropy in photogeneration in these devices. Inability to find a good rectifying, planar contact was also a limiting factor. Here we report the observation of high photoconductive gain in planar geometry photodiodes based on aligned nanoribbons of PBTTT and discuss the origin of the high photoconductivity anisotropy with field direction along the polymer chain and perpendicular to the polymer chains.

2. Experimental

2.1. Device fabrication

To fabricate the in-plane photodiodes, PBTTT (M_n = 25.6 kg mol^{-1}, M_w = 46.8 kg mol^{-1}, PDI = 1.83) was dissolved in anhydrous 1,2-dichlorobenzene by annealing at 110 °C for 30 min to obtain a 2 mg/mL solution in nitrogen atmosphere. The PBTTT films were zone-cast inside a nitrogen glovebox on top of precleaned (sonication in acetone, IPA followed by oxygen plasma treatment) glass substrates (Corning 1737F). The details of the zone-casting parameters have been reported previously [13]. Next, the zone-cast film was annealed inside the glovebox at 275 °C on a preheated hotplate for 2–3 s to induce nanoribbons. As soon as the polymer melts, which can be detected by the change in color (from dark red to transparent) of the polymer film, the hotplate was turned off to allow slow cooling of the substrate below 80 °C. The annealing time was kept short in order to avoid the dewetting of the polymer on the glass substrate. Despite a slightly wavy pattern of the nanoribbons caused by the variation in polymer chain length, significant optical dichroism with dichroic ratio of 6 was achieved in these films. Thirty nanometer thick top gold contacts were evaporated through a TEM grid, used as shadow mask, to define a planar photodiode with a 20 μm channel length and a width of 1 mm. In order to avoid sample-to-sample variation, devices with different orientation of the electrodes were fabricated on the same substrate. The AFM image in Fig. 1 shows the surface roughness of the zone-cast film of around 15 nm which is typically much higher than that of spin coated films.

2.2. Measurement

All the measurements were done in a vacuum environment at a base pressure of 10^{-6} mbar. External quantum efficiency measurements were performed using both unpolarized, CW and pulsed optical excitation. The spot size for CW excitation was 457 μm × 585 μm, while for pulsed measurement it was 1.33 mm × 1.35 mm. Spot size was measured using a beam profiler (WinCamD-UCD12, DataRay Inc.). Illumination was from the top side, hence the Au electrodes acted as masks. Since the device area 20 μm × 1 mm was less than the spot size, appropriate correction was made while calculating the gain factor. For pulsed excitation an unpolarized green LED (532 nm) light source was driven using a function generator and

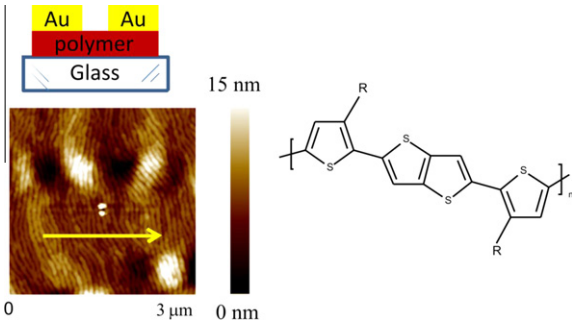

Fig. 1. Chemical structure of C14-PBTTT (R = $C_{14}H_{29}$) (right) and device structure (top left), glass/zone-cast PBTTT (120 nm)/Au (30 nm). Device area was 0.02 mm^2. AFM image of the zone-cast film annealed at 275 °C to induce nanoribbon phase (bottom left). The arrow is showing the zone-casting direction.

the resultant photocurrent transient was measured using a preamplifier and oscilloscope combination with 50 Ω coupling resistance. Typical bias applied in this case was 200 V (field $\sim 10^5$ V/cm) using a Keithley 6517B electrometer. The intensity of the pulsed excitation was measured using a calibrated Si photodiode (Thorlabs SM05PD1A).

3. Results and discussions

3.1. Characterization of planar diode

The dark current–voltage (I_{dark}–V) characteristics of the top contact devices were carried out both in a nitrogen filled glovebox and in vacuum (base pressure of 10^{-6} mbar). The magnitude of I_{dark} was slightly higher in the N_2-glovebox probably due to some residual doping by moisture and oxygen. The I_{dark}–V characteristics in vacuum (Fig. 2a and b) show a sizable anisotropy in I_{dark} magnitude consistent with our previous measurement in transistors [13]. When the polymer chains are aligned along the direction of current flow, i.e., when the PBTTT nanoribbons, resolved in the AFM images, are perpendicular to the current flow, the current is by around a factor of 5 higher than when the polymer chains are oriented perpendicular to the direction of current flow. (I_{dark}–V) characteristics were also measured on bottom contact devices (PBTTT zone cast on top of photolithographically defined Au electrodes with channel length 20 μm). In this case the I_{dark} values did not reproducibly show a large anisotropy. This might suggest that the alignment at the bottom interface is perturbed by the presence of Au electrodes which have a different surface energy compared to the glass substrate. Therefore top contact geometry was selected for all the measurements reported below.

These devices were further characterized by external quantum efficiency measurement (EQE) under continuous illumination (Fig. 2a and b) with different applied bias. The measured EQE values at voltages >80 V (0.4×10^5 V/cm) exceed 100% and increase with increasing bias. Clearly these devices are operating in photoconductive gain regime [14–17]. The EQE given by the ratio of number of charge carriers collected in the external circuit and number of photons incident onto the device active area per second ($=I_{ph}hc/q\lambda P$), from now on called as Gain (G), shows anisotropy ~10 at voltages ⩽150 V (0.75×10^5 V/cm) for chain orientation parallel and perpendicular to the direction of current flow. We further measured the CW intensity dependence of G which shows a strong decrease with increasing the intensity of illumination, varying from 1000 at 5 μW to ~95 at 110 μW of CW excitation (Fig. 2e). We also investigated the gain characteristics of asymmetric top contact (Au–Al) devices. However, the dark current values in forward and reverse bias were similar to those of Au–Au top contact devices. Consequently similar Gain values were achieved in asymmetric electrode devices.

Photoconductive gain can be caused by trapping of one type of charge carriers (electron) and the consequent increase in carrier recombination lifetime (τ). If the transit time of the free carrier (hole) $t_{tr} \ll \tau$, the injected hole per photogenerated electron will be transported across the device many more times before recombining with the electron [14–17]. This gives rise to an enhancement in the measured quantum efficiency, $G \propto \tau/t_{tr}$. An alternative model for photomultiplication mechanism given by Reynaert et al. assumes exciton mediated detrapping of holes from deep trap states to shallow trap levels [18]. These detrapped holes will eventually be trapped into the deep trap levels again however the time required to return to the equilibrium is longer than the transit time of these non-relaxed holes. Photomultiplication is thus caused by injection and transport of these non-equilibrium holes.

In our case the most likely mechanism for photoconductive gain is trapping of the photogenerated electrons in the bulk of the semiconductor due to less efficient electron transport in PBTTT (FETs based on PBTTT with Ca source–drain, exhibit poor electron transport with low mobility of $\sim 7 \times 10^{-4}$ cm^2/V s, while with Au source–drain no electron current was detected) [19]. Although we fabricated our films under N_2 atmosphere and measured them in vacuum the origin of photoconductive gain and electron trapping could be electrochemical reaction with residual moisture and oxygen in the films. The other common origin for long-lived electron traps can be residual chemical impurities either present in the polymer or introduced inside the glovebox during the film forming process.

The anisotropy observed in G can be attributed to the difference in t_{tr} resulting from the anisotropy in mobility. Charge injection from the ohmic electrodes (Au) could also play a role in determining the anisotropy, as the injection current has been found to be proportional to the mobility in the bulk [20]. Hence, when the field is oriented perpendicular to polymer chains, due to lower mobility in the channel and/or less effective injection of holes the transit time decreases, giving rise to a lower G. The intensity dependence of the CW-gain can be related to intensity dependent decrease in the recombination lifetime due to "filling up" of the deep trap states. This aspect will be discussed in detail in the following section.

3.2. Transient photocurrent response under pulsed illumination

The charge trapping effect becomes more evident upon shining light for several minutes and then turning it off. After switching off the light, the photocurrent relaxes quite slowly with an apparent persistent behavior and the sample only recovers to the dark conditions over a period of several minutes. The long tail over which the photocurrent decays to its dark value is due to the slow thermal release of electrons from the deep trap states and subsequent recombination with free holes. This extremely slow decay indicates the trapping and release of electrons from the deep trap states takes place over several minutes (Fig. 2f).

The transient response of these planar photodiodes was recorded under pulsed illumination ($\omega \sim 10$ Hz, 532 nm) with varying intensity (Fig. 3a and b). The photocurrent rise and decay kinetics at the short timescale of 100 ms can thus be understood due to the trapping and detrapping of electrons from shallow trap states with thermal release rate, $\tau_{rel}^{-1} > \omega$.

Fig. 3a and b shows the normalized transient response with intensity as a parameter. Under low intensity of

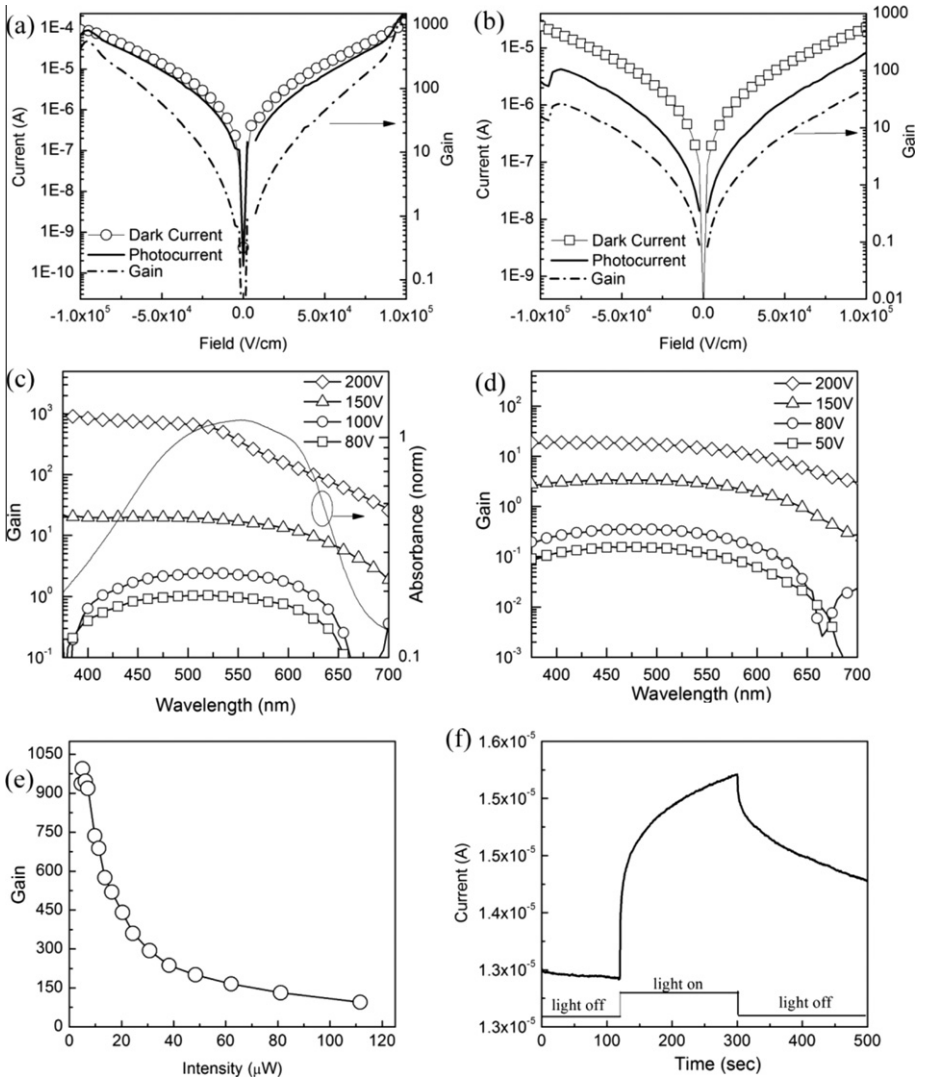

Fig. 2. Bias dependence of dark current, photocurrent (light–dark) and gain for field orientation parallel (a) and perpendicular (b) to polymer chains. Device was illuminated by ~5 μW light of wavelength 530 nm. The gain-spectrum with field orientation parallel (c) and perpendicular (d) to polymer chains at different bias under ~5 μW intensity of illumination. (e) CW intensity dependence of the Gain with a constant bias 200 V applied across the electrode. Field was directed parallel to polymer chains. For field oriented perpendicular to the polymer chains, a similar trend is observed; (f) Light induced persistent photoconductivity under a bias voltage of 150 V. The device was illuminated using ~5 μW, 530 nm light. (For interpretation of the references to colour in this figure legend, the reader is referred to the web version of this article.)

illumination ($\leqslant$10.7 mW/cm^2), photocurrent builds up slowly and does not saturate to a steady state value. As the intensity increases beyond 10.7 mW/cm^2 the photoresponse becomes faster, a steady state is achieved within the 100 ms light irradiation and the rise and decay curves with different, sufficiently high intensity tend to overlap on each other. The decay of the photocurrent exhibits two distinct time constants. We detect a fast decay component (over which the photocurrent decays to 50% of the steady state value), which grows in magnitude as the intensity increases. In contrast, the slope of the slow decay component (51–100 ms) remains constant.

If the trapping time, τ_t, is shorter than the free carrier recombination lifetime, τ_n, $\tau_t < \tau_n$, so that electrons experience trapping prior to recombination with holes, rise time and decay time (t_{res}) is given by, $t_{res} \approx (1 + n_t/n)\tau_n$, where n the free electron density and n_t is the electron density in the shallow trap states [21]. At higher intensities the density of free electrons is enhanced with respect to the density of trapped electrons and this is the reason why the rise and decay is faster at high intensity than at low intensity. Above a certain intensity (>10.7 mW/cm^2) a steady state photocurrent is achieved and a thermal equilibrium between free electrons and electrons in shallow traps is established. Under that condition n_t/n can be expressed in terms of the Boltzmann ratio = N_t/N_0 exp(ΔE/kT), where N_t is the density of trap states in an energy level ΔE below the band edge and N_0 is the density of free states

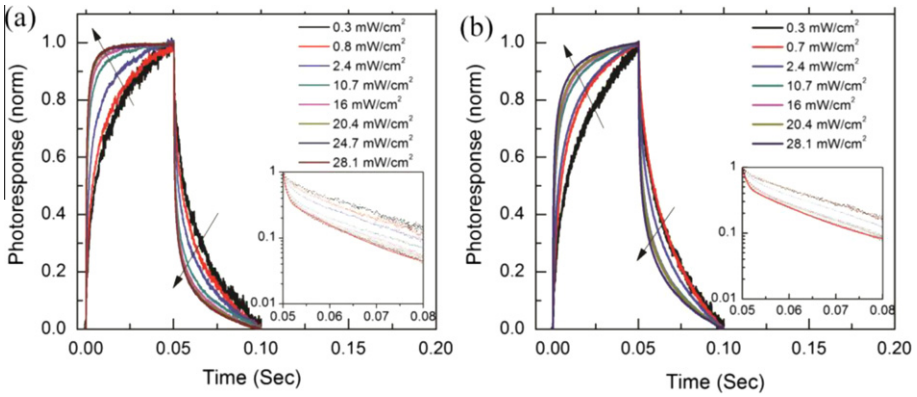

Fig. 3. Normalized photocurrent transients measured in a top-contact device using 50 ms square light pulse from a green LED of varying intensity. (a) Field parallel (perpendicular) to polymer chains (nanoribbons). (b) Field perpendicular (parallel) to polymer chains (nanoribbons). Photocurrent decay has been plotted in the inset in log-linear scale. The solid red line is the biexponential fit to the data (dotted lines). (For interpretation of the references to colour in this figure legend, the reader is referred to the web version of this article.)

at the band edge. Clearly, as this ratio does not depend on intensity, the rise and decay time will be a constant multiple of τ_n and will be independent of intensity. This also explains the saturation of G observed at higher intensity.

The photocurrent decay was fitted using a double exponential function (Fig. 3a and b inset) which reveals two distinct time constants: the fast decay immediately after switching off the light followed by a slow decaying tail over several milliseconds. Fast decay time constants of $\sim$500 μs for field parallel to polymer chains and $\sim$700 μs for field perpendicular to polymer chains were obtained at the highest light intensity. The slow decay component exhibits similar time constant of $\sim$12 ms for both orientations and might be due to release of electrons from deeper traps. The fast decay component can be due to (1) actual collection of free holes and (2) recombination of free holes with electrons detrapped from shallow trap states. The fast decay component is still much slower than the transit time calculated using hole mobilities obtained from transistor measurement (with $\mu_h^{\parallel} \sim 0.1$ cm^2/V s, transit time = $L^2/\mu V = 0.1$ μs, where $L = 20$ μm is the length of the channel, $V = 200$ V is the applied bias). However, the high hole mobility measured in the FETs can arise due to filling up of the traps and high density of charge in the channel induced by gate voltage. In the ungated planar photodiodes the hole mobility could be significantly lower.

The gain value, calculated by measuring the amplitude of the transient photocurrent modulation and the intensity of the light pulse by a calibrated photodiode, was $\sim$10 at 110 μW of pulse intensity, which is significantly lower than for CW illumination of comparable light intensity. This difference in gain values suggests that in the pulsed illumination experiment only a quasi-steady state has been reached, there is in fact a further, slow rise of photocurrent over longer time scales building up to the value measured under CW conditions.

3.3. Effect of background illumination

Next, we studied the transient behavior exposing the devices to a short light pulse while continuously illuminating the device with a strong CW illumination. A constant background illumination helps to maintain a constant population in the trap states and a small amplitude pulse does not perturb the electron trap population significantly, hence the resultant transient was expected to be less affected by electron trapping effects [22,23].

Fig. 4a and b shows the effect of increasing the background illumination on transients recorded for a fixed 5 μW pulse illumination. The amplitude of the photocurrent pulse decreases with increasing background intensity. With a background illumination $\geqslant$155 μW (= 8.6 mW/cm^2) steady state condition is achieved in conjunction with faster rise and decay. Hence a 155 μW background intensity is sufficient to raise the free electron density and fill up deep traps so that the rise and decay kinetics for a 5 μW pulse is less affected by deep traps and becomes faster. Also the decreasing current magnitude indicates that the gain is being suppressed by filling up the traps with the background illumination. Transients recorded with varying pulse intensity for a fixed background illumination (155 μW) are presented in Fig. 4c and d. As depicted in the insets, normalized transients for different pulse intensities overlap.

Even though charge trapping effects can be reduced using background illumination, the photoconductive gain mechanism is still active. G measured for the pulsed illumination was $\sim$10 and 4 for fields parallel and perpendicular to the polymer chain direction, respectively. In the previous section, a two trap level viz. deep and shallow trap picture, with two different and well separated time constants for trapping, has been adapted. With the background illumination it is likely that we fill the deep trap states. The slow rise in the photocurrent observed during continuous illumination (Fig. 1f) suggests that the time required to reach the equilibrium population in the deep trap levels is indeed long. Electrons photogenerated due to the additional pulse illumination will not interact with the deep trap states. The residual gain observed here is mainly due to recombination with shallow electron trap states.

3.4. PBTTT–C_{60} bilayer devices

Identifying electron trapping as the dominant mechanism for high photoconductive gain, we introduced an

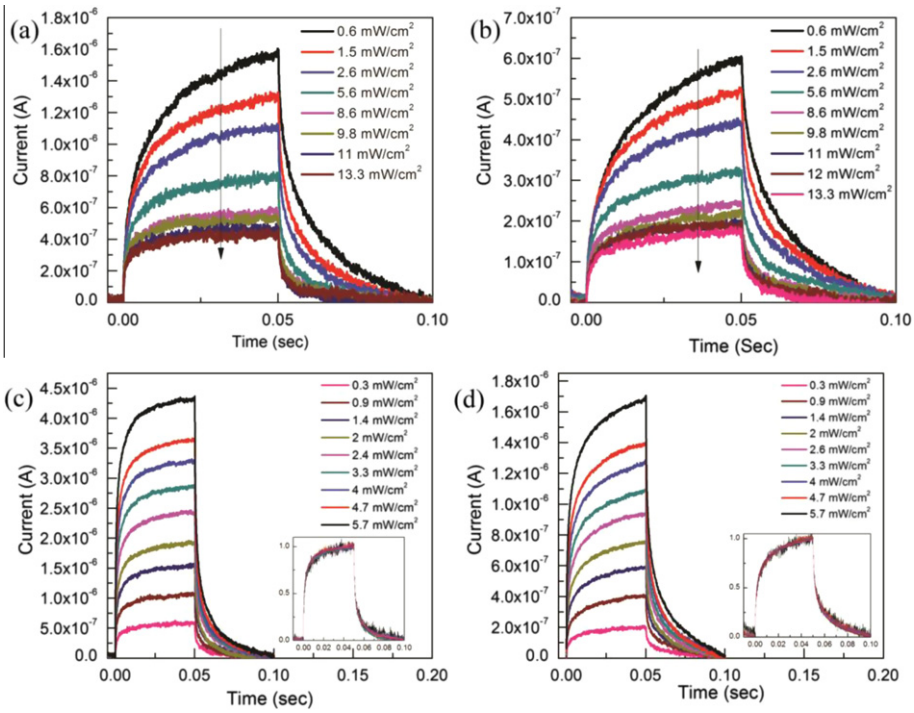

Fig. 4. (a and b) Photocurrent transients for a small amplitude (5 μW) pulse with varying background CW illumination intensity. Field orientation is (a) parallel and (b) perpendicular to polymer chains. (c and d) Photocurrent transients for a fixed background light intensity (155 μW) and varying pulse intensity with field (c) parallel and (d) perpendicular to polymer backbone. Insets graphs showing the normalized photocurrent transients which overlap.

electron acceptor layer of C_{60} on the surface of the PBTTT film to reduce gain effects by providing an efficient pathway for extracting electrons from the device. We fabricated a bi-layer device where 40 nm C_{60} was evaporated on top of the PBTTT layer without affecting the alignment of the polymer.

Fig. 5 shows the *I–V* characteristics for the PBTTT/C_{60} planar diodes with Au and Al top contact. The dark current under reverse bias (positive voltage applied to Al electrode) is reduced to 1 μA as compared to pristine case, $I_{dark} \sim 100$ μA at 10^5 V/cm. Forward bias current also decreases in magnitude suggesting a overall decrease in hole mobility presumably due to interpenetration of C_{60} into the polymer. Measured *G* value under reverse bias mode was 0.7 and 0.06 (corresponding to EQE values of 70% and 6% with 10^5 V/cm applied field) for field parallel and perpendicular to polymer chains respectively. Similar EQE value was reported for MEHPPV–PCBM blend [24] whereas much lower EQE of 4% was reported in P3HT–PCBM blend based planar photodiodes [25]. This suggests that despite lower electron trapping and decreased hole mobility photoconductive gain mechanism might still be active in this system and bulk doping of PBTTT with C_{60} is required without disturbing the alignment.

It is encouraging to reduce *G* below 1 by incorporating C_{60}, but it also prevents us to estimate the charge generation efficiency in pristine PBTTT since exciton dissociation

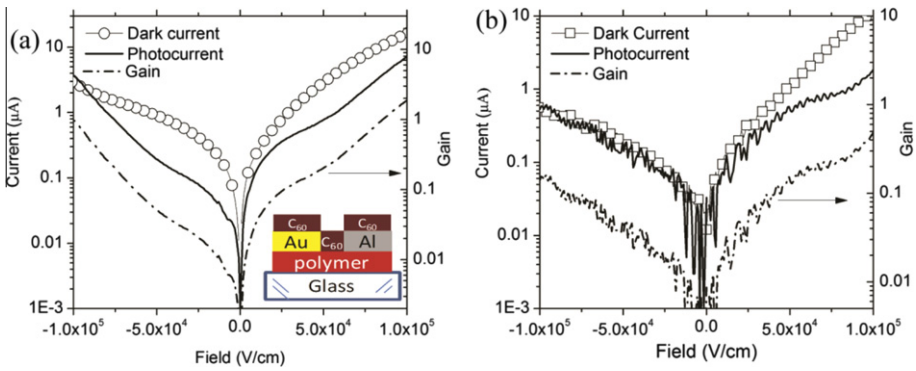

Fig. 5. Dark current and photocurrent (light–dark) versus voltage for field applied parallel (a) and perpendicular to the polymer chains. Device schematic is shown in the inset. Devices were illuminated using 200 μW, 532 nm light source. The calculated gain value is also shown (dotted).

at the PBTTT–C_{60} interface is highly efficient and recombination losses are minimal. Hence other polyfluorene-based acceptor-type copolymers, such as poly((9, 9-dioctylfluorene)-2,7-diyl-alt-[4,7-bis(3-hexylthien-5-yl) -2,1,3-benzothiadiazole]-2′,2″-diyl) (F8TBT), poly(dioctylfluorene-co-benzothiadiazole) (F8BT) might be a better choice where lower charge generation efficiency at the interface is expected owing to insufficient energy offset at the heterojunction and enhanced geminate recombination. In such system one might hope to see significant improvements of device performance over what is possible in the conventional sandwich geometry.

4. Conclusion

We have carried out a comparative study of photoconductivity of PBTTT thin film with two different orientation of the external field viz. parallel and perpendicular to the polymer chains. Photocurrent measured under low level light intensity indicates a large photoconductive gain due to dominant electron trapping in the bulk. Anisotropy in the measured gain indicates anisotropy in the hole transit time, consistent with the mobility anisotropy measured in this system. Transient photocurrent measurements reveal the presence of deep and shallow trap levels with well separated time constant for trapping and detrapping. A constant background illumination was used to fill up the deep trap states and reduce the photoconductive gain by decreasing recombination lifetime of the carriers. Formation of a bilayer heterojunction with a C_{60} electron-acceptor layer was effective to reduce EQE below 100%. Although high photoconductive gain observed in PBTTT based planar diodes poses a challenge in terms of measuring the intrinsic photogeneration anisotropy in this system it can be utilized to design efficient photodetectors for imaging applications.

Acknowledgment

We acknowledge financial support from the Engineering and Physical Sciences Research Council (EPSRC). D.G. thanks Prof. Neil Greenham, Dr. Matt Bird and Dr. Mario Caironi for useful discussions.

References

[1] S.H. Park, A. Roy, S. Beaupre, S. Cho, N. Coates, J.S. Moon, D. Moses, M. Leclerc, K. Lee, A.J. Heeger, Bulk heterojunction solar cells with internal quantum efficiency approaching 100%, Nat. Photonics 3 (2009) 297–303.
[2] C.R. McNeill, A. Abrusci, J. Zaumseil, R. Wilson, M.J. McKiernan, J.H. Burroughes, J.J.M. Halls, N.C. Greenham, R.H. Friend, Dual electron donor/electron acceptor character of a conjugated polymer in efficient photovoltaic diodes, Appl. Phys. Lett. 90 (2007) 193506.
[3] D. Gupta, D. Kabra, N. Kolishetti, S. Ramakrishnan, K.S. Narayan, An efficient bulk-heterojunction photovoltaic cell based on energy transfer in graded-bandgap polymers, Adv. Funct. Mater. 17 (2007) 226–232.
[4] B. Sun, E. Marx, N.C. Greenham, Photovoltaic devices using blends of branched CdSe nanoparticles and conjugated polymers, Nano Lett. 3 (2003) 961–963.
[5] D. Veldman, S.C.J. Meskers, R.A.J. Janssen, The energy of charge-transfer states in electron donor–acceptor blends: insight into the energy losses in organic solar cells, Adv. Funct. Mater. 19 (2009) 1939–1948.
[6] Y. Zhou, K. Tvingstedt, F. Zhang, C. Du, W.-X. Ni, M.R. Andersson, O. Inganäs, Observation of a charge transfer state in low-bandgap polymer/fullerene blend systems by photoluminescence and electroluminescence studies, Adv. Funct. Mater. 19 (2009) 3293–3299.
[7] J. Piris, T.E. Dykstra, A.A. Bakulin, P.H.M. van Loosdrecht, W. Knulst, M. Tuan Trinh, J.M. Schins, L.D.A. Siebbeles, Photogeneration and ultrafast dynamics of excitons and charges in P3HT/PCBM blends, J. Phys. Chem. C 113 (2009) 14500–14506.
[8] J. Guo, H. Ohkita, H. Benten, S. Ito, Near-IR femtosecond transient absorption spectroscopy of ultrafast polaron and triplet exciton formation in polythiophene films with different regioregularities, J. Am. Chem. Soc. 131 (2009) 16869–16880.
[9] J. Zaumseil, C. Groves, J.M. Winfield, N.C. Greenham, H. Sirringhaus, Electron–hole recombination in uniaxially aligned semiconducting polymers, Adv. Funct. Mater. 18 (2008) 3630–3637.
[10] C. Groves, N.C. Greenham, Bimolecular recombination in polymer electronic devices, Phys. Rev. B 78 (2008) 155205.
[11] I. McCulloch, M. Heeney, C. Bailey, K. Genevicius, I. MacDonald, M. Shkunov, D. Sparrowe1, S. Tierney, R. Wagner, W. Zhang, M.L. Chabinyc, R.J. Kline, M.D. McGehee, M.F. Toney, Liquid-crystalline semiconducting polymers with high charge-carrier mobility, Nat. Mater. 5 (2006) 328–333.
[12] D.M. DeLongchamp, R.J. Kline, Y. Jung, D.S. Germack, E.K. Lin, A.J. Moad, L.J. Richter, M.F. Toney, M. Heeney, I. McCulloch, Controlling the orientation of terraced nanoscale "Ribbons" of a poly(thiophene) semiconductor, ACS Nano 3 (2009) 780–787.
[13] M.J. Lee, D. Gupta, N. Zhao, M. Heeney, I. McCulloch, H. Sirringhaus, Anisotropy of charge transport in a uniaxially aligned and chain-extended, high-mobility, conjugated polymer semiconductor, Adv. Funct. Mater. 2011.
[14] I.H. Campbell, B.K. Crone, Bulk photoconductive gain in poly(phenylene vinylene) based diodes, J. Appl. Phys. 101 (2007) 024502.
[15] J.C. Ho, A. Arango, V. Bulović, Lateral organic bilayer heterojunction photoconductors, Appl. Phys. Lett. 93 (2008) 063305.
[16] M. Binda, T. Agostinelli, M. Caironi, D. Natali, M. Sampietro, L. Beverina, R. Ruffo, F. Silvestri, Fast and air stable near-infrared organic detector based on squaraine dyes, Org. Electron. 10 (2009) 1314–1319.
[17] G. Konstantatos, E.H. Sargent, PbS colloidal quantum dot photoconductive photodetectors: transport, traps and gain, Appl. Phys. Lett. 91 (2007) 173–505.
[18] J. Reynaert, V.I. Arkhipov, P. Heremans, J. Poortmans, Photomultiplication in disordered unipolar organic materials, Adv. Funct. Mater. 16 (2006) 784–790.
[19] N. Zhao, Field effect transistors based on microcrystalline conjugated polymer, Ph.D. Thesis, University of Cambridge, 2008.
[20] Y. Shen, M.W. Klein, D.B. Jacobs, J.C. Scott, G. Malliaras, Mobility-dependent charge injection into an organic semiconductor, Phys. Rev. Lett. 86 (2001) 3867.
[21] R. Bruggemann, Analysis of photoconductive decay from a trapping perspective, Solid State Commun. 101 (1997) 199–203.
[22] C.R. McNeill, I. Hwang, N.C. Greenham, Photocurrent transients in all-polymer solar cells: trapping and detrapping effects, J. Appl. Phys. 106 (2009) 024507.
[23] I. Hwang, C.R. McNeill, N.C. Greenham, Drift-diffusion modeling of photocurrent transients in bulk heterojunction solar cells, J. Appl. Phys. 106 (2009) 094506.
[24] A.C. Niemeyer, I.H. Campbell, F. So, B.K. Crone, High quantum efficiency polymer photoconductors using interdigitated electrodes, Appl. Phys. Lett. 91 (2007) 103504.
[25] M. Caironi, T. Agostinelli, D. Natali, M. Sampietro, R. Cugola, M. Catellani, S. Luzzati, External quantum efficiency versus charge carriers mobility in polythiophene/methanofullerene based planar photodetectors, J. Appl. Phys. 102 (2007) 024503.